Self-cleaning, photocatalytic films on aluminum plates for multi-pollutant air remediation: promoting adhesion and activity by SiO_2 interlayers

Self-cleaning, photocatalytic films on aluminum plates for multi-pollutant air remediation: promoting adhesion and activity by SiO_2 interlayers

Carolina Cionti[a,b,§], Ewoud Cosaert[c,§], Gabriele Deshayes[a], Ermelinda Falletta[a,b], Daniela Meroni [a,b,*], Claudia L. Bianchi[a,b,*], Dirk Poelman[c,*]

[a] *Università degli Studi di Milano, Department of Chemistry, Milan, Italy*

[b] *Consorzio INSTM, Florence, Italy*

[c] *Ghent University, Department of Solid State Sciences, Ghent, Belgium*

§ *These authors contributed equally to this work.*

* *Corresponding authors:* daniela.meroni@unimi.it; claudia.bianchi@unimi.it; dirk.poelman@ugent.be

Abstract

In recent years, nanoparticles have come under close scrutiny for their possible health and environmental issues, making them less attractive for photocatalytic applications in air or water purification. Replacing free nano-powders with active and stable films is thus a fundamental step towards developing effective photocatalytic devices. Aluminum represents a cheap and technologically-relevant substrate, but its photocatalytic applications have been hampered by adhesion issues and metal ion diffusion within the photocatalytic layer. In this work, the use of silica interlayers is investigated as a strategy to promote adhesion, efficiency and reusability of TiO_2 films deposited on aluminum plates. Films were prepared from stable titania sols to avoid the use of nano-powders. Aluminum substrates with different surface morphology were investigated and the role of the silica interlayer thickness was studied. Films were extensively characterized, studying their structure, morphology, optical properties, adhesion and hardness. Self-cleaning properties were studied with respect to their superhydrophilicity and ability to resist fouling via alkylsilanes. Photocatalytic degradation tests were carried out using both volatile organic compounds (VOC) and NOx, also in recycle tests. The presence of the silica interlayer proved crucial to promote the film

robustness and photocatalytic activity. The substrate morphology determined the optimal interlayer thickness, especially in terms of the film reusability.

Keywords

photocatalytic oxidation, smart coatings, self-cleaning, nitrogen oxides, air pollution, indoor pollution

1. Introduction

Nanostructured powders have recently come under increased public and regulatory scrutiny for their possible health effects and environmental fate[1–3]. While most of the literature on photocatalysis has so far involved free nanostructured powders, the preparation of stable and active photocatalytic macroscopic structures is regarded as a key step towards developing effective photocatalytic devices with good recyclability. In this respect, film deposition on a variety of substrates is one of the most investigated approaches, especially on glass[4,5], ceramics[6,7], titanium[8,9] and steel[10,11]. Aluminum substrates are economical, lightweight, versatile, electrically conductive and are widely applied in numerous technologies. Photocatalytic coatings on aluminum supports could be beneficial especially for advanced technologies, such as combined treatments with non-thermal plasma[12], where aluminum electrodes are generally adopted. Localized surface plasmon resonance (LSPR)[13] using the LSPR properties of aluminum[14,15] can also be used to promote the activity. However, the application of aluminum as substrate for photocatalytic devices has been limited due to several issues. In particular, previous reports have shown a detrimental effect of aluminum substrates with respect to other supports, such as quartz and stainless steel[16,17], which was attributed to the diffusion of aluminum ions within the photocatalytic layer, where they acted as charge recombination centers. This effect can be compared to the detrimental effects of sodium diffusion from soda lime substrates at elevated temperature[18]. Moreover, cracked and flaky morphologies have been observed for photocatalytic layers deposited on aluminum substrates, possibly due to thermal stress arising from mismatch in thermal expansion coefficients[19], leading to poor reusability of the films[20]. In order to promote adhesion, composites with organic binders are often employed[21,22], which are generally susceptible to photocatalytic oxidation, or require expensive and complex deposition techniques, such as atomic layer deposition[20,23] or spray pyrolysis[24]. The use of compatibility layers based on alumina has also be reported[22], which promotes adhesion but does not solve the issue of aluminum ion diffusion.

As a result, TiO_2 films on aluminum substrates are currently mainly proposed as simple anticorrosion coatings[25]. The photocatalytic application of TiO_2 film deposited on aluminum substrate is more limited and generally related to application in aqueous phase and, in many cases, deposition procedures involve the use of nanopowders[26,27].

In this work, titania films were deposited, by a simple spin coating procedure, on aluminum substrates with different surface morphologies, starting from a stable sol without the addition of preformed nanoparticles. For the sake of comparison, TiO_2 films on glass were also prepared. In order to promote the adhesion to the metal substrate and to limit metal ion diffusion within the photocatalyst layers, the role of a silica interlayer of varying thickness was investigated. The

morphology, mechanical stability and photocatalytic performance were evaluated, also in recycle tests, showing a key role of the silica interlayer thickness. The films photoactivity was tested towards two classes of air pollutants, nitrogen oxides and VOC: for the latter class, ethanol was chosen as model volatile organic compound. Ethanol is a key primary pollutant emitted by a wide variety of biogenic and anthropogenic sources, such as fermentation processes, biofuel production and usage, and consumer products[28]. Furthermore, ethanol has been extensively used as model alcohol in both theoretical and experimental studies[29,30] thanks to its relatively simple molecular structure (it contains only two carbon atoms), which however still retains a C-C bond, making its chemistry more similar to that of longer hydrocarbon chains than 1C models. Nitrogen oxides (*i.e.* NO and NO_2) are ubiquitous air pollutants usually produced by fuels' combustion and are known for affecting the ozone layer as well as for being greenhouse gasses. Finally, the reusability of the films was also tested, with results supporting a main role of the silica interlayer.

2. Experimental section

All reagents were purchased from Sigma Aldrich, unless specified otherwise, and Milli-Q water was used for the preparation of solutions and suspensions.

2.1. Film preparation

Both aluminum plates and Pyrex glass substrates (5x5 cm^2) were adopted as substrates. Aluminum laminas were either used as obtained or roughened using TP41-P80 sandpaper before use.

Prior to deposition, glass and aluminum substrates were cleaned by subsequent sonication in acetone, 2-propanol and water and dried in an oven at 150°C overnight. All aluminum laminas were also etched in a 10%w oxalic acid solution at 80 °C for 1 hour, while glass substrates were immersed in concentrated sulfuric acid, then rinsed with water.

For selected samples, an intermediate SiO_2 layer, deposited from a stable silica sol, was added to improve adhesion and reduce the diffusion of substrate ions within the titania layer. The silica sol was prepared at room temperature using the following procedure[31]: 4.9 mL of tetraethyl orthosilicate was mixed with 16.8 mL of water, 25.4 mL of ethanol and 2.2 mL of HCl 1 M. The mixture was magnetically stirred for 1 hour and then aged for 24 hours. Silica films were deposited with a spin coater (SPIN 150, SPS) using a spinning time of 20 s, spinning rate of 3000 rpm and acceleration of 500 rpm/s. A varying number of layers was deposited (up to 6). After the consecutive deposition of three layers, samples were placed in an oven at 80°C overnight to promote densification of the film.

The TiO_2 films were deposited starting from a stable titania sol, prepared according to a previously reported procedure[5]. Briefly, the TiO_2 sol was prepared at room temperature: 1.0 mL of HCl 37% (12 mmol) was mixed with 160 mL of a 0.6 M titanium isopropoxide solution in ethanol. Then, as a stabilizer, 0.47 g of a non-ionic surfactant, Lutensol ON70 (BASF), was added to the sol after being dissolved in 130 mL of ethanol. The reaction mixture was stirred at room temperature for 1 hour with a magnetic stirrer. Before deposition, the TiO_2 sol was diluted 1:2 with ethanol. Titania layers were deposited by spin coating using the same conditions reported for silica film, then the film was immediately calcined at 400 °C for 1 h under O_2 flux (heating ramp of 12.5 °C min^{-1}, 9 NL h^{-1}) to promote crystallization and adhesion.

Samples were named as *ZSxTy*, where *Z* is the used substrate (Al for as obtained aluminum laminas, *Al for sand-papered aluminum substrates, and none for glass substrates), *x* is the number of deposited SiO_2 layers (3,6 or none) and *y* indicates the number of titania layers. Table 1 lists the prepared samples.

Table 1. List of the prepared samples, indicating the type of substrate and the number of silica and titania layers.

Sample name	Substrate	SiO_2 layers	TiO_2 layers
T3	Pyrex glass	-	3
S3T3	Pyrex glass	3	3
S6T3	Pyrex glass	6	3
*AlT3	Sand-papered aluminum	-	3
*AlS3T3	Sand-papered aluminum	3	3
*AlS6T3	Sand-papered aluminum	6	3
AlS3T3	As-obtained aluminum	3	3
AlS6T3	As-obtained aluminum	6	3

2.2. Characterization methods

Optical total transmission spectra of the coatings on glass and diffuse reflection spectra of the samples on aluminum were both investigated using a UV-vis-NIR spectrophotometer (PerkinElmer Lambda 1050S), equipped with a spectralon-coated integrating sphere.

X-ray diffraction patterns were collected on a Bruker D5000 diffractometer working with Cu Kα radiation (λ = 0.154 nm, 40 kV, 40 mA).

Scanning electron microscopy (SEM) images were obtained on FEI Quanta200F equipped with EDX (EDAX genesis 4000) and on a JSM-IT500 LV (JEOL).

Contact angles were measured with a Krüss Easydrop Standard instrument and DSA1 software.

Spectroscopic ellipsometry measurements were performed using a J.A.Woollam M-2000 system in order to obtain an estimate of the thickness of the coatings, using an angle of incidence of 75°. CompleteEASE software (Woolam) was used to analyze the data. Measurements were carried out on different points of the sample to evaluate the coating thickness homogeneity and average values were determined. Ellipsometry data were fitted using a Cauchy refractive index model for the TiO_2 layer, including a correction for surface roughness.

The film hardness was measured with a scratch test according to the Wolff Wilborn method. A TQC VF2378 kit, operating in accordance with the ISO 15184 standard, was adopted. The hardness scale, from soft to hard, is the following: 6B 5B 4B 2B B HB F H 2H 3H 4H 5H 6H 7H 8H 9H.

Adhesion tests were performed with a TQC CC3000 instrument according to the ISO 2409:2013 standard. Two series of parallel cuts cross angled to each other were made with the test kit to obtain a pattern of squares. After applying an adhesion tape and shortly after removing it, the integrity of the ruled area was evaluated by optical assessment and SEM images (Hitachi TM-1000 equipped with EDX probe).

Film roughness was evaluated as arithmetic mean deviation of the primary profile (Pa) via profilometry measurements by using a DektakXT (Bruker) instrument.

2.3. Self-cleaning tests

The self-cleaning properties of the films were investigated via two types of tests: superhydrophilic behavior and tests of anti-fouling performance, both carried out under UV light irradiation (Jelosil HG500 lamp, effective irradiation power: 30 mW cm^{-2}).

UV-induced hydrophilic properties were tested by measuring the static contact angle of water droplets on the prepared films as a function of irradiation time.

Anti-fouling tests were performed by purposely fouling the film surface with alkylsilanes through chemical vapor deposition, according to a previously reported procedure[5]. Siloxanes are air pollutants present in many consumer products[32], which react with the surface of TiO_2 photocatalysts and impair their photocatalytic activity[33,34], hence tests with alkylsilanes were carried out to simulate the photocatalyst deactivation. After the film fouling, the samples where irradiated with UV light and the anti-fouling capacity was evaluated via water contact angle measurements.

2.4. Gas-phase photocatalytic tests

The photocatalytic activity of the films was evaluated by stress tests towards two classes of air pollutants (VOC and nitrogen oxides).

Photocatalytic abatement of ethanol (Merck) was analyzed in a custom-made stainless steel tube reactor with a volume of 8.75 L, using a previously described setup[35]. During the reaction the atmosphere was stirred with a fan and kept at 40 °C, in order to avoid temperature fluctuations due to the light source and the environment. After evacuating the reactor, an Ar/O_2 (ration 80:20) gas mixture was added up to 1050 mbar to represent atmospheric air and 6 µL of ethanol was injected (273 ppm). The thin films were illuminated at a distance of 15 cm at 100 W with the light of a focused mercury high-pressure short arc bulb (Osram HBO 200 W/2). The gas inside the reactor chamber was continuously analyzed using a quadrupole mass spectrometer (Pfeiffer Vacuum GSD 301 C2) during the abatement of ethanol, obtaining signals from Ar, O_2, CO_2 and ethanol (40 amu, 32 amu, 44 amu and 45 amu respectively).

The mineralization degree was calculated according to the following equation:

$$mineralization\ degree = \frac{2 \cdot C_{0,EtOH} - C_{t,CO_2}}{2 \cdot C_{0,EtOH}} \cdot 100$$

where $C_{0,EtOH}$ is the initial concentration of ethanol and C_{t,CO_2} is the concentration of the produced CO_2 at time *t* of irradiation.

The photocatalytic removal of nitrogen oxides (NO_x) was tested in a Pyrex glass cylindrical reactor with a 20 L of effective volume. Tests were carried out under UV light irradiation, using a halogenide lamp (Jelosil HG500, 500 W) emitting in the 340–400 nm wavelength range and yielding an effective irradiation power on the film surface of 20 mW cm^{-2}. The sample irradiated area was 50 mm x 33 mm. Tests were performed at 25 °C, with a starting NOx concentration of (1000±50) ppb. The NO and NO_2 concentrations were monitored using an on-line chemiluminescence analyzer (ENVEA AC32e).

Recycle tests were performed on the best performing samples to evaluate their reusability. Before reusage the films were irradiated with UV light.

3. Results and discussion

Photocatalytic titania films were prepared on glass and aluminum substrates with or without the presence of silica interlayers.

Figure 1 reports the XRD patterns of the films deposited over three layers of silica on glass substrates and aluminum laminas. The XRD pattern of *AlT3 sample is also reported as reference. The patterns of the samples with six silica interlayers are reported in Figure S1. All samples exhibit peaks characteristic of anatase TiO_2[36] in good agreement with previous results[37]. Besides the anatase peaks, all of the reflections appreciable in the diffraction patterns of the films deposited on aluminum plates are due to the substrate, as clearly appreciable from the diffractogram of the bare

aluminum lamina (Figure S1). The XRD patterns of S3T3 and S6T3 samples show an amorphous halo due to the glass substrate. Due to the large roughness of the substrates and the low TiO_2 layer thickness, the signal to noise ratio of the XRD patterns was limited and no accurate crystallite sizes could be deduced from the XRD patterns. Using the Scherrer equation, estimated crystallite sizes were of the order of 20 nm, in accordance with previous works from our group[37].

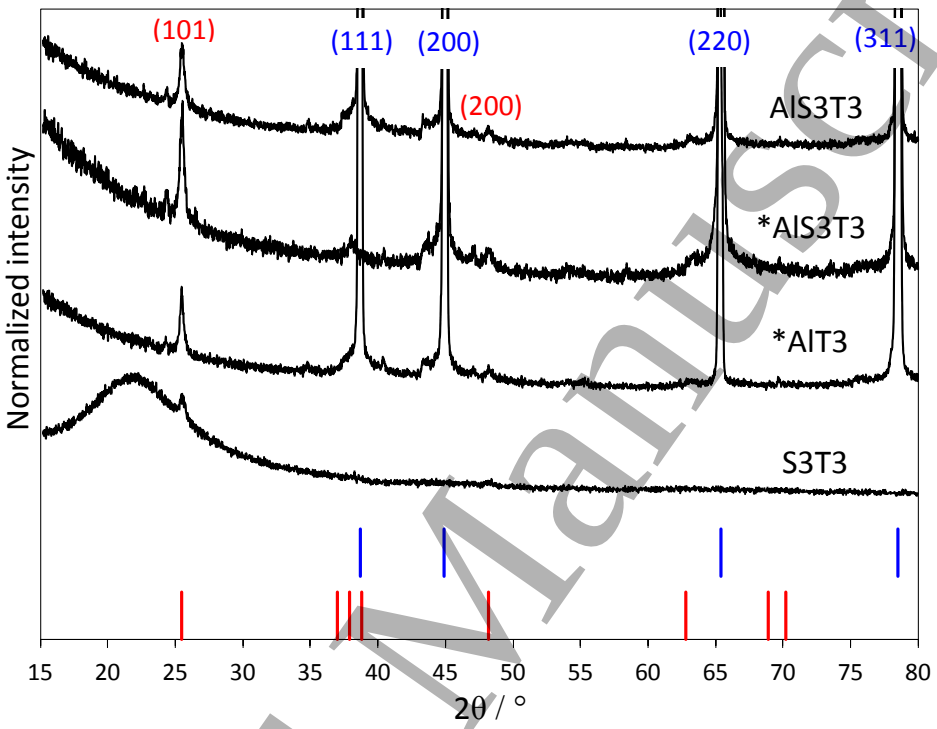

Figure 1. XRD patterns of composite films with three silica layers on glass, as-obtained and sand-papered aluminum substrates. The red and blue lines indicate the characteristic patterns of anatase TiO_2[36] and *fcc* Al[38,39], respectively.

The thickness of the TiO_2 films was estimated by ellipsometry. Measurements were carried out solely on films deposited on glass substrates, since the large surface roughness of the aluminum substrate prevented reliable measurements. All samples exhibited similar value of thickness of the TiO_2 film: (130 ± 20) nm, (120 ± 10) nm and (120 ± 10) nm for T3, S3T3 and S6T3, respectively. The thickness of the silica layer could not be measured by ellipsometry, but it was previously evaluated by cross-sectional SEM images on glass substrates to be *ca.* 100 nm per spin-coated layer[31].

The morphology of the films was evaluated using scanning electron microscopy. Figure 2 reports the SEM images of titania films on glass, as-obtained and sand-papered aluminum, with three or six silica interlayers. The images without silica interlayer are reported in Figure S2. Marked differences

are appreciable among the tested substrates. Glass substrates present homogeneous and continuous coatings, without appreciable cracks, both in the case of the T3 (Figure S2a) and the S3T3 samples (Figure 2a), whereas the addition of further silica interlayers leads to cracking, owing to the thick films internal stress[40], and to partial detachment of the titania layer (S6T3, Figure 2d). Aluminum plates present a rougher morphology with respect to glass substrates: the etching treatment yields the formation of a highly porous surface, with micro-scale roughness. In the case of sand-papered films, a more irregular morphology is obtained, characterized by grooves along with micrometric porosity. The direct deposition of a titania layer on this aluminum substrate leads to an inhomogeneous coating (Figure S2b), as confirmed by EDX spectra, with appreciable cracks, especially within substrate grooves. The addition of a silica interlayer presents a beneficial effect on the morphology of films deposited on aluminum laminas, but the two types of aluminum substrates show notable differences in terms of the optimal number of silica interlayers. In the case of the as-obtained laminas (Figure 2b, e), highly homogeneous coatings are observed upon the addition of three silica layers, whereas introducing a thicker interlayer leads to cracking of the film. This is also confirmed by SEM images of the same substrates coated with only silica layers (before titania deposition), reported in Figure S3c,d. While the film morphology is highly homogeneous after the deposition of three layers of silica, further silica deposition results in the formation of surface aggregates, indicative of an excess of deposited oxide. On the contrary, titania coatings on sand-papered aluminum (Figure 2c, f) exhibit an opposite trend, with a better film quality showed by the *AlS6T3 sample with respect to the *AlS3T3. Higher resolution images (Figure S3) show that the titania coating covers the rough aluminum substrate in a homogeneous way, although in the case of *AlT3S3 a few film imperfections and cracks are visible. Moreover, the underling rough structure of the aluminum substrate is more appreciable in the *AlS3T3 sample, in agreement with the thinner silica interlayer. In both cases nanometric spherical features are appreciable, which can be attributed to small aggregates of titania nanoparticles. In this respect, silica films on sand-papered substrate before titania deposition (Figure S4a,b) show a homogeneous coating even after the deposition of six layers, with no surface aggregates to suggest excess deposition. Therefore, the increased roughness imparted by the sand-papering treatment (Pa values from profilometry measurements: 0.31 and 2.31 for Al and *Al, respectively) requires a thicker silica interlayer to stabilize the film adhesion on the aluminum substrate. It is noteworthy that the surface roughness values of films onto sand-papered aluminum present a trend in good agreement with SEM findings: Pa values of 2.66, 3.82 and 0.91 were measured for, respectively, *AlT3, *AlS3T3 and *AlS6T3. Therefore, *AlT3 presents a surface roughness quite comparable with the bare *Al substrate, while the *AlS3T3 shows the higher roughness possibly due to the cracks and other film defects observed

in SEM images. Conversely, *AlS6T3 shows much lower surface roughness with respect to the bare substrate which can be attributed to a flattening property of the silica interlayer.

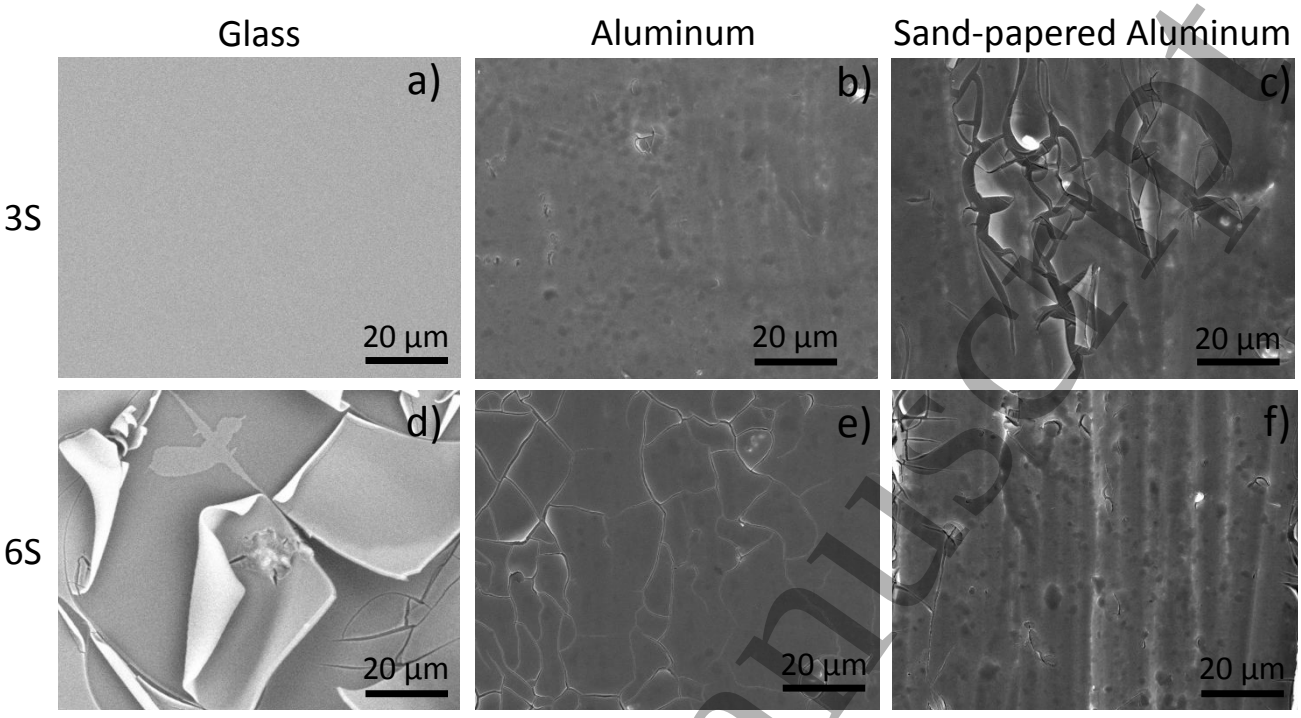

Figure 2. SEM images of composite films with three (a,b,c) and six (d,e,f) silica interlayers on different substrates: glass (a,d), aluminum (b,e), sand-papered aluminum (c,f).

The mechanical properties of the films on sand-papered aluminum were evaluated in terms of the hardness and adhesion. The films' hardness was carried out by Wolff Wilborn method, showing for all samples a value of F, which is a medium hardness value, in close agreement with the performance of the pristine substrate. Adhesion was evaluated by comparing SEM images of the films before and after crisscrossing the film with a razor blade and applying and removing an adhesive tape. Figure S5 shows that all the tested samples retained the titania layer after adhesion test. However, the films' morphology appears smoother, particularly in *AlT3 and *AlS3T3, due to the loss of the cracked outer layer of the coating. Overall, the *AlS6T3 sample, which showed a better starting film morphology, was the least affected by the adhesion test.

The optical properties of the films were investigated by UV-vis spectroscopy, as reported in Figure S6. Films deposited on glass (Figure S6a) show interference fringes in the 350-700 nm region, characteristic of thin titania films[41] and retains a good degree of transparency with respect to the pristine glass substrate. The addition of silica interlayer leads to a slight decrease in the transparency of the film, more marked for the S6T3 sample, in good agreement with the lower homogeneity of the latter observed in SEM images. The reflectance of films deposited on aluminum substrates (Figure S6b) shows, with respect to the bare substrate, the absorption characteristics of

the deposited oxides in the UV region. Sand-papered aluminum samples showed lower reflectance in the whole spectrum which could be mainly related to scattering effects due to the increased surface roughness caused by the substrate pre-treatment.

The self-cleaning properties of the films were studied with respect to the UV-induced superhydrophilic properties as well as the anti-fouling behavior towards alkylsilanes. Figure 3a reports the superhydrophilicity tests of films with three layers of silica, whereas the tests on samples with six layers of silica are reported in Figure S7. Before irradiation, all films exhibited a hydrophilic behavior, with contact angles ranging from *ca.* 50° for samples on glass and as-obtained aluminum, to *ca.* 30° of coatings on sand-papered aluminum. This difference in wettability can be attributed to the surface roughness of the substrates: rougher surfaces promoted hydrophilicity as explained by the classical Wenzel model[42]. After irradiation, samples on glass and smooth aluminum substrates reached a complete water spreading after 25 minutes, whereas films on roughened aluminum became superhydrophilic within only 5 minutes. Ho and co-authors reported superior photoinduced hydrophilic property for aluminum-supported titania films with respect to films deposited on quartz and stainless steel[16]: they attributed this behavior to higher surface roughness and increased surface hydroxylation of aluminum-supported films. Our results point towards a main effect of surface roughness in promoting the light-induced superhydrophilic behavior of aluminum-based films.

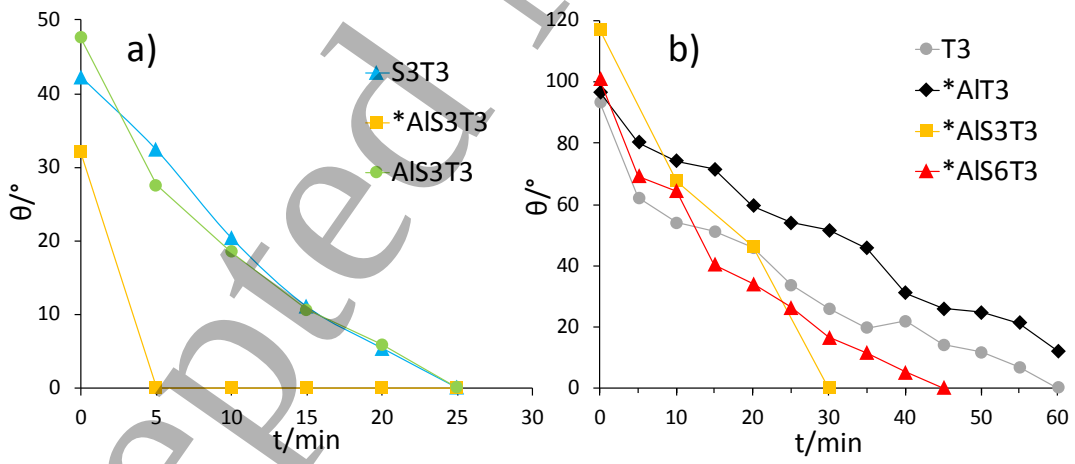

Figure 3. a) Water contact angle as a function of irradiation time of titania films deposited on different substrates and with three silica layers; b) Water contact angle as a function of irradiation time during anti-fouling tests of films deposited on sand-papered aluminum; the curve of T3 sample deposited on glass is also reported as a reference. Estimated standard deviation ± 5°.

The films' ability to regenerate their surface state by UV irradiation after fouling was investigated using alkylsilanes. Siloxanes were selected to simulate the photocatalyst deactivation, as they are air

pollutants present in many consumer products[32] able to react with the surface of TiO_2 photocatalysts and impair their photocatalytic activity[33,34]. Figure 3b compares the anti-fouling tests of films on sand-papered aluminum with respect to the T3 reference. After fouling with long-alkyl-chain moieties, hydrophobic water contact angles were measured for all the investigated samples; the highest angle was observed for *AlS3T3, in agreement with its higher surface roughness. Upon irradiation, the photocatalytic degradation of the silane alkyl chains take place, resulting in a decrease of the observed contact angle until complete water spreading is observed when the surface hydroxylation is fully restored. The TiO_2 film deposited on glass reached complete water spreading in 1 hour, whereas the *AlT3 sample did not reach complete self-cleaning in the investigated timescale. The composite films on aluminum substrates exhibited much better performance, reaching complete self-cleaning within less than 50 min, with the *AlS3T3 being the fastest. Figure S8 reports the water contact angle images during superhydrophilicity and anti-fouling tests of *AlS3T3.

The photocatalytic activity of films was also tested towards the degradation of a model pollutant in stress tests. The degradation of ethanol was measured by monitoring both pollutant removal and CO_2 formation, as the result of complete mineralization. Ethanol disappearance follows a pseudo-zero-order kinetics; rate constants were determined in the first 120 min and the relative values are reported in Table 2, along with the mineralization degree after 210 min irradiation, obtained from CO_2 released percentage. Similarly to what was observed in self-cleaning tests, films on glass supports displayed a slower reaction kinetics, both in terms of pollutant disappearance and mineralization degree with respect to the coatings on aluminum. The only exception to this general trend is *AlT3, which represents the worst performing film, supporting the occurrence of metal ion migration within the TiO_2 layer. In this respect, it should be noted that among the glass samples, the T3 film displays lower photocatalytic activity than S3T3 and S6T3, suggesting a beneficial effect of the silica interlayer, possibly related to the suppression of alkali metal ion migration from the glass support. Overall, the best performing samples are composite films on sand-papered aluminum, possibly as a result of their rougher surface which could endow a larger contact area. While both aluminum substrates show a slight decrease in the rate constant of ethanol increasing the number of silica layers, the mineralization degree shows a significant increase, especially in the case of the *AlS6T3 film.

Table 2. Pseudo-zero-order rate coefficients, *k*, and mineralization degree at 3.5 h of irradiation from ethanol photocatalytic degradation tests. The estimated standard deviation is $\pm$ 0.01$\cdot$ 10^{-7} M s^{-1} for the rate coefficients and $\pm$ 2% for the mineralization.

k· 10^{-7} ($M\ s^{-1}$)			
Substrate	**n° SiO_2 layers**		
	0	**3**	**6**
Glass	3.92	4.68	4.36
Aluminum	-	5.01	4.65
Sand-papered Aluminum	0.60	5.33	5.03

% mineralization			
Substrate	**n° SiO_2 layers**		
	0	**3**	**6**
Glass	21	37	33
Aluminum	-	45	48
Sand-papered Aluminum	7	49	61

Recycle tests were carried out on the two best performing samples, *AlS3T3 and *AlS6T3, and are reported in Figure 4a. While the activity of two samples is comparable in the initial tests, the performance of *AlS3T3 starts to decline at the third run, whereas *AlS6T3 better retains its activity. Notably, the same conclusion could be drawn from repeated tests on a different pollutant, NO_x. Figure 4b shows the NO_x concentration as a function of irradiation time during recycle tests: the NO_x concentration takes into account both the NO and NO_2 species. Figure S9 reports a representative example of NO and NO_2 concentrations during irradiation: while NO shows a bell-shaped profile characteristic of reaction intermediates, the concentration of the more toxic NO_2 is directly abated. When comparing recycle tests, it is noteworthy that, even if the *AlS3T3 sample presents slightly higher activity than *AlS6T3 in the first run, its performance shows a marked decrease within the consecutive cycles. The improved reusability of *AlS6T3 can be explained by considering its more homogeneous morphology, testified by SEM images, and good adhesion promoted by the thicker silica interlayer.

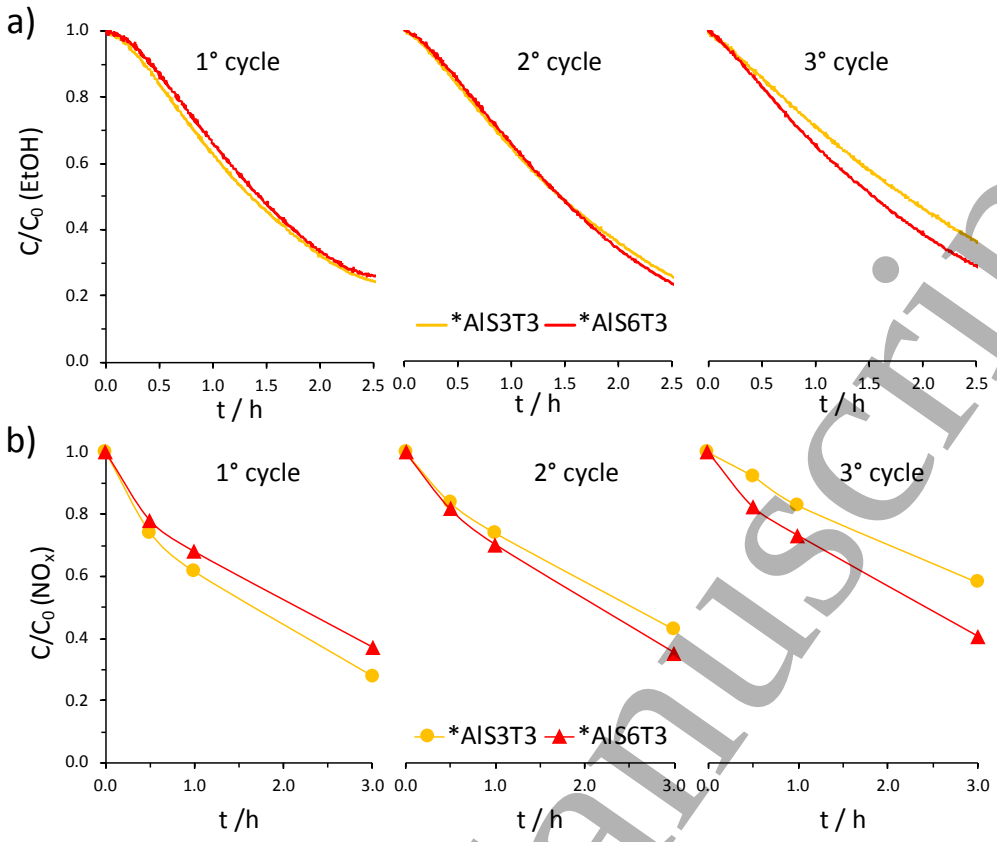

Figure 4. Photocatalytic removal of ethanol (a) and NOx (b): reusability of films deposited on sand-papered aluminum.

Overall the rate coefficient k of *AlS3T3 is slightly higher than the one of *AlS6T3, while the latter sample is characterized by a markedly higher mineralization degree (as reported in Table 2). The higher k value of *AlS3T3 can be attributed to a larger degree of ethanol adsorption due to the rougher surface morphology of this sample with respect to *AlS6T3 (as shown by contact angle and profilometry measurements). On the other hand, the presence of six silica interlayers in *AlS6T3 sample lowers the surface roughness, but also increases the mineralization degree and reusability of the film. These beneficial effects in *AlS6T3 can be attributed to a lower metal ion diffusion within the photocatalytic film and to an increase in the coating stability.

Conclusions

The use of aluminum plates as photocatalytic substrates presents notable challenges: the formation of cracked and flaky layers was observed when titania coatings were directly deposited on aluminum laminas. Moreover, these films exhibited very poor photocatalytic performance, attributable to aluminum ion diffusion within the titania lattice.

We demonstrated that silica films can act as a compatibility layer for the deposition of stable and reusable photocatalytic TiO_2 coatings on aluminum substrates. This approach improves the morphology of the resulting film, without the need of resorting to complex and expensive deposition procedures. In addition, the photocatalytic performance was markedly promoted, supporting an effective suppression of metal ion diffusion within the titania layer. In this respect, the addition of a silica interlayer proved beneficial also for borosilicate glass substrates, which are known to be prone to the diffusion of alkali metal ions. This approach can thus be extended to a variety of technologically relevant substrates, elevating common materials to cost-effective alternative to materials such as quartz, sodium-free glass and titanium.

The nature of the substrate and its surface roughness determined the optimal number of silica layers to be introduced. When the silica interlayer was too thin, moderate cracking was still observed, whereas a too thick silica interlayer led to peeling off of the film. The use of rougher surfaces, as in the case of sand-papered aluminum, required a higher number of silica layers, possibly to promote a more homogeneous surface where the nanometric titania coating could effectively adhere.

However, the addition of a thicker silica layer did not erase the effect of the sand-paper pretreatment on surface roughness. Films on sand-papered substrates showed promoted photocatalytic activity with respect to the smoother counterparts, possibly due to their larger exposed contact area.

The prepared films showed excellent UV-induced superhydrophilicity, anti-fouling properties with respect to known poisoning agents, such as siloxanes, and photocatalytic activity towards different classes of indoor and outdoor air pollutants. Finally, by modulating the silica interlayer thickness, the mechanical stability and reusability of the films could be effectively promoted.

Acknowledgements

Dr. Daniele Marinotto at SmartMatLab (UNIMI) and Dr Stefania Crespi at the Department of Earth Sciences “Ardito Desio” (UNIMI) are kindly acknowledged for profilometry measurements and SEM images, respectively. G.D. acknowledges financial support from the Erasmus+ program. This work was financially supported by the BOF Special Research Fund from Ghent University, GOA project no. 01G00319.

References

1. Paterson, G., Ataria, J. M., Hoque, M. E., Burns, D. C. & Metcalfe, C. D. The toxicity of titanium dioxide nanopowder to early life stages of the Japanese medaka (Oryzias latipes). *Chemosphere* **82**, 1002–1009 (2011).
2. Pozzo, R. L., Baltanás, M. A. & Cassano, A. E. Supported titanium oxide as photocatalyst in

water decontamination: State of the art. *Catal. Today* **39**, 219–231 (1997).
3. Camera-Roda, G. & Santarelli, F. Optimization of the thickness of a photocatalytic film on the basis of the effectiveness factor. *Catal. Today* **129**, 161–168 (2007).
4. Cerrato, G. *et al.* Micro-TiO2 coated glass surfaces safely abate drugs in surface water. *J. Hazard. Mater.* **363**, 328–334 (2019).
5. Antonello, A., Soliveri, G., Meroni, D., Cappelletti, G. & Ardizzone, S. Photocatalytic remediation of indoor pollution by transparent TiO2 films. *Catal. Today* **230**, 35–40 (2014).
6. Martins, M. A. *et al.* Preparation and photocatalytic activity of chemically-bonded phosphate ceramics containing TiO2. *Appl. Surf. Sci.* **404**, 18–27 (2017).
7. Rimoldi, L., Meroni, D., Cappelletti, G. & Ardizzone, S. Green and low cost tetracycline degradation processes by nanometric and immobilized TiO 2 systems. *Catal. Today* **281**, 38–44 (2017).
8. Zhao, L. na, Jia, Y. H., You, H., Wang, S. tao & Fu, L. Photocatalytic performance and application outlook of 3D TiO2/titanium mesh modified by GO-Ag joined-deposition. *Catal. Today* **340**, 106–114 (2020).
9. Li, D., Zhang, X. & Zhang, W. Designing a new reaction system by stacking use of Ti mesh supported Ag/N-TiO2 nano-sheets for enhanced photocatalytic degradation of bisphenol A. *Chem. Eng. J.* **405**, 126867 (2021).
10. Bianchi, C. L., Pirola, C., Selli, E. & Biella, S. Photocatalytic NOx abatement: The role of the material supporting the TiO2 active layer. *J. Hazard. Mater.* **211**–**212**, 203–207 (2012).
11. Murgolo, S. *et al.* A new supported TiO 2 film deposited on stainless steel for the photocatalytic degradation of contaminants of emerging concern. *Chem. Eng. J.* **318**, 103–111 (2017).
12. Saoud, W. A. *et al.* Synergism between non-thermal plasma and photocatalysis: Implicationsin the post discharge of ozone at a pilot scale in a catalytic fixed-bed reactor. *Appl. Catal. B Environ.* **241**, 227–235 (2019).
13. Mesbah, M. *et al.* Synergistic enhancement of photocatalytic antibacterial effects in high-strength aluminum/TiO2 nanoarchitectures. *Ceram. Int.* **46**, 24267–24280 (2020).
14. Ghori, M. Z. *et al.* Role of UV Plasmonics in the Photocatalytic Performance of TiO 2 Decorated with Aluminum Nanoparticles. *ACS Appl. Nano Mater.* **1**, 3760–3764 (2018).
15. Li, Z. *et al.* Drastic enhancement of photoelectrochemical water splitting performance over plasmonic Al@TiO2 heterostructured nanocavity arrays. *Nano Energy* **51**, 400–407 (2018).
16. Ho, W., Yu, J. C. & Lee, S. Photocatalytic activity and photo-induced hydrophilicity of mesoporous TiO2 thin films coated on aluminum substrate. *Appl. Catal. B Environ.* **73**, 135–143 (2007).
17. Cai, X., Ren, Z., Hu, T. & Xie, Y. Interface diffusion and reaction between TiO2 film photocatalyst and aluminium alloy substrate. *Surf. Interface Anal.* **32**, 218–223 (2001).
18. Tomaszewski, H. *et al.* Effect of Substrate Sodium Content on Crystallization and Photocatalytic Activity of TiO 2 Films Prepared by DC Magnetron Sputtering. *Int. J. Photoenergy* **2007**, 1–5 (2007).
19. Lopez, L., Daoud, W. A., Dutta, D., Panther, B. C. & Turney, T. W. Effect of substrate on surface morphology and photocatalysis of large-scale TiO 2 films. *Appl. Surf. Sci.* **265**, 162–168 (2013).
20. Levchuk, I. *et al.* Photocatalytic activity of TiO2 films immobilized on aluminum foam by atomic layer deposition technique. *J. Photochem. Photobiol. A Chem.* **328**, 16–23 (2016).
21. Seabra, M. P., Rego, E., Ribeiro, A. & Labrincha, J. A. Photodegradation of Orange II solutions by TiO2 active layers jet sprayed on aluminium sheets. *Chem. Eng. J.* **171**, 175–180 (2011).
22. Wang, X., Han, F., Wang, X. & Li, Y. Effect of aluminum foam support and polyethylene glycol on surface morphology and photocatalytic behavior of TiO2 films. *Mater. Chem. Phys.* **145**, 68–74 (2014).

23. Dias, V. *et al.* Atomic Layer Deposited TiO2 and Al2O3 Thin Films as Coatings for Aluminum Food Packaging Application. *Materials (Basel).* **12**, 682 (2019).
24. Stambolova, I., Shipochka, M., Blaskov, V., Loukanov, A. & Vassilev, S. Sprayed nanostructured TiO2 films for efficient photocatalytic degradation of textile azo dye. *J. Photochem. Photobiol. B Biol.* **117**, 19–26 (2012).
25. Liu, T., Zhang, F., Xue, C., Li, L. & Yin, Y. Structure stability and corrosion resistance of nano-TiO2 coatings on aluminum in seawater by a vacuum dip-coating method. *Surf. Coatings Technol.* **205**, 2335–2339 (2010).
26. Liu, J. *et al.* Cold Spray Construction of Nanostructured Titania Coatings for Photocatalytic Applications. *J. Therm. Spray Technol.* (2021). doi:10.1007/s11666-021-01167-1
27. Tasbihi, M., Kete, M., Raichur, A. M., Tušar, N. N. & Štangar, U. L. Photocatalytic degradation of gaseous toluene by using immobilized titania/silica on aluminum sheets. *Environ. Sci. Pollut. Res.* **19**, 3735–3742 (2012).
28. Millet, D. B. *et al.* Natural and Anthropogenic Ethanol Sources in North America and Potential Atmospheric Impacts of Ethanol Fuel Use. *Environ. Sci. Technol.* **46**, 8484–8492 (2012).
29. Zhong, L. & Haghighat, F. Modeling of by-products from photocatalytic oxidation (PCO) indoor air purifiers: A case study of ethanol. *Build. Environ.* **144**, 427–436 (2018).
30. Hansen, J. Ø. *et al.* Unravelling Site-Specific Photo-Reactions of Ethanol on Rutile TiO2(110). *Sci. Rep.* **6**, 21990 (2016).
31. Rimoldi, L. *et al.* Three-dimensional mesoporous silica networks with improved diffusion and interference-abating properties for electrochemical sensing. *Electrochim. Acta* **291**, 73–83 (2018).
32. Genualdi, S. *et al.* Global Distribution of Linear and Cyclic Volatile Methyl Siloxanes in Air. *Environ. Sci. Technol.* **45**, 3349–3354 (2011).
33. Pazokifard, S., Mirabedini, S. M., Esfandeh, M., Mohseni, M. & Ranjbar, Z. Silane grafting of TiO 2 nanoparticles: dispersibility and photoactivity in aqueous solutions. *Surf. Interface Anal.* **44**, 41–47 (2012).
34. Zhao, J., Milanova, M., Warmoeskerken, M. M. C. G. & Dutschk, V. Surface modification of TiO2 nanoparticles with silane coupling agents. *Colloids Surfaces A Physicochem. Eng. Asp.* **413**, 273–279 (2012).
35. Meroni, D. *et al.* Photocatalytic removal of ethanol and acetaldehyde by N-promoted TiO2 films: The role of the different nitrogen sources. *Catal. Today* **161**, 169–174 (2011).
36. Cionti, C., Della Pina, C., Meroni, D., Falletta, E. & Ardizzone, S. Photocatalytic and Oxidative Synthetic Pathways for Highly Efficient PANI-TiO2 Nanocomposites as Organic and Inorganic Pollutant Sorbents. *Nanomaterials* **10**, 441 (2020).
37. Soliveri, G. *et al.* Self-cleaning properties in engineered sensors for dopamine electroanalytical detection. *Analyst* **140**, 1486–1494 (2015).
38. Gazanfari, M. *et al.* Synthesis of aluminium nanoparticles by arc evaporation of an aluminium cathode surface. *Bull. Mater. Sci.* **37**, 871–876 (2014).
39. Ayieko, C. O. *et al.* Controlled Texturing of Aluminum Sheet for Solar Energy Applications. *Adv. Mater. Phys. Chem.* **05**, 458–466 (2015).
40. Wang, X., Xiong, R. & Wei, G. Preparation of mesoporous silica thin films on polystyrene substrate by electrochemically induced sol–gel technique. *Surf. Coatings Technol.* **204**, 2187–2192 (2010).
41. Maino, G. *et al.* Electrochemically assisted deposition of transparent, mechanically robust TiO2 films for advanced applications. *J. Nanoparticle Res.* **15**, 2087 (2013).
42. Drelich, J., Chibowski, E., Meng, D. D. & Terpilowski, K. Hydrophilic and superhydrophilic surfaces and materials. *Soft Matter* **7**, 9804 (2011).